Action-Potential Modulation During Axonal Conduction

Takuya Sasaki,[1] Norio Matsuki,[1] Yuji Ikegaya[1,2]*

Once initiated near the soma, an action potential (AP) is thought to propagate autoregeneratively and distribute uniformly over axonal arbors. We challenge this classic view by showing that APs are subject to waveform modulation while they travel down axons. Using fluorescent patch-clamp pipettes, we recorded APs from axon branches of hippocampal CA3 pyramidal neurons ex vivo. The waveforms of axonal APs increased in width in response to the local application of glutamate and an adenosine A_1 receptor antagonist to the axon shafts, but not to other unrelated axon branches. Uncaging of calcium in periaxonal astrocytes caused AP broadening through ionotropic glutamate receptor activation. The broadened APs triggered larger calcium elevations in presynaptic boutons and facilitated synaptic transmission to postsynaptic neurons. This local AP modification may enable axonal computation through the geometry of axon wiring.

Contrary to the prevailing notion of the digital-like uniformity of action potentials (APs), recent evidence has shown that APs (or axons) are capable of conveying information in a graded analog manner (*1*–*4*). It remains unknown, however, whether already-generated APs can be modulated during axonal conduction. Because axons express various types of transmitter receptors and ion channels, in particular on their presynaptic terminals (*5*, *6*), local alterations in the ion conductance of aligned synapses along an axon may modify the waveforms of APs traveling down its length.

We recorded CA3 pyramidal cells (PCs) in hippocampal slice cultures, unless otherwise specified (*7*). Alexa Fluor–loaded patch pipettes were used to visualize their axons (Fig. 1A). An axonal branch that was 150 to 700 μm away from the axon hillock was targeted for cell-attached recording with a fluorophore-coated pipette under spinning-disk confocal visualization (*8*). APs were evoked by current injection into the soma and were extracellularly captured at the axon as sharp sink potentials. Extracellularly recorded APs (eAPs) were likely to be a mixture of the inverse of intracellularly recorded APs (iAPs) and their derivatives (fig. S1).

Glutamate or γ-aminobutyric acid (GABA) was locally puff-applied to the axon midway between two patch-clamp pipettes. The effective radius of this local application was less than 100 μm, as confirmed by diffusion of coapplied Alexa Fluor dye. Application of 10 μM glutamate induced a rapid and reversible increase in the half-maximal duration of eAPs that were recorded within 200 μm of the site of glutamate administration (Fig. 1B, $t_{10} = 5.44$, $P = 0.0003$ paired t test). This low concentration of glutamate did not change the iAP width recorded at the soma (Fig. 1B, –0.61 ± 1.6%, $t_{10} = 0.28$, $P = 0.78$) or the somatic resting membrane potential (–0.4 ± 0.8 mV of change, $t_{10} = 0.53$, $P = 0.60$). It also did not affect the spike activity of nearby neurons (fig. S2). Unlike glutamate, 1 mM GABA had no significant effect on the eAP width (Fig. 1C, $t_5 = 1.03$, $P = 0.34$).

Glutamate did not broaden eAPs in the presence of 10 μM 6-cyano-7-nitroquinoxaline-2,3-dione (CNQX), a non–*N*-methyl-D-aspartate (NMDA) receptor antagonist (Fig. 1C, $t_6 = 1.31$, $P = 0.23$), but it did in the presence of 50 μM L,D-2-amino-5-phosphonopentanoic acid (AP5), an NMDA receptor antagonist (MCPG) (Fig. 1C, $t_5 = 3.47$, $P = 0.02$), and 500 μM (*S*)-α-methyl-4-carboxyphenylglycine, a group I/II metabotropic glutamate receptor antagonist (Fig. 1C, $t_5 = 7.42$, $P = 0.0006$). The eAP broadening was not affected by bath application of a glutamate transporter inhibitor [100 μM DL-threo-β-benzyloxyaspartic acid (TBOA)] (Fig. 1C, $t_3 = 4.00$, $P = 0.028$), preincubation with a vesicle fusion inhibitor [10 nM tetanus toxin (TeNT)] (Fig. 1C, $t_4 = 4.06$, $P = 0.0097$), or intracellular injection of a Ca^{2+} chelator [20 mM 1,2-bis(*o*-aminophenoxy)ethane-*N*,*N*,*N*',*N*'-tetraacetic acid (BAPTA)] into the somata (Fig. 1C, $t_3 = 4.19$, $P = 0.024$). Thus, glutamate appears to

[1]Laboratory of Chemical Pharmacology, Graduate School of Pharmaceutical Sciences, University of Tokyo, Tokyo 113-0033, Japan. [2]Precursory Research for Embryonic Science and Technology, Japan Science and Technology Agency, 4-1-8 Honcho Kawaguchi, Saitama 332-0012, Japan.

*To whom correspondence should be addressed. E-mail: ikegaya@mol.f.u-tokyo.ac.jp

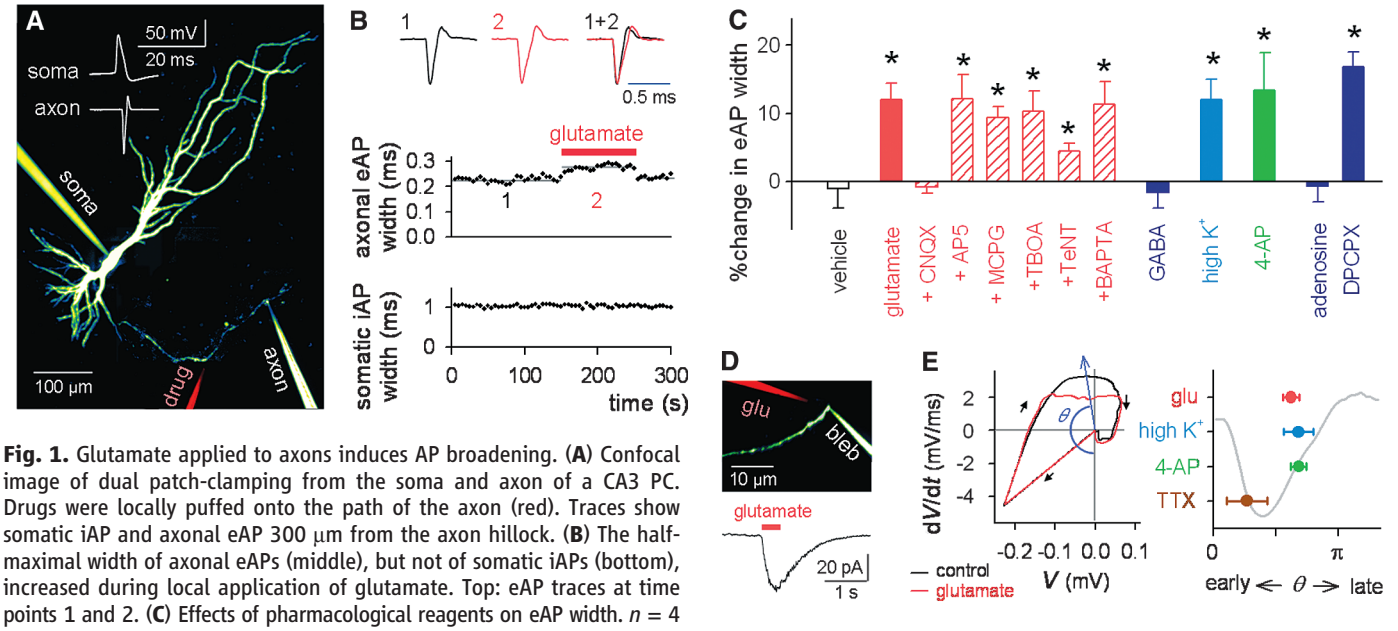

Fig. 1. Glutamate applied to axons induces AP broadening. (**A**) Confocal image of dual patch-clamping from the soma and axon of a CA3 PC. Drugs were locally puffed onto the path of the axon (red). Traces show somatic iAP and axonal eAP 300 μm from the axon hillock. (**B**) The half-maximal width of axonal eAPs (middle), but not of somatic iAPs (bottom), increased during local application of glutamate. Top: eAP traces at time points 1 and 2. (**C**) Effects of pharmacological reagents on eAP width. $n = 4$ to 7 slices, $^*P < 0.05$, paired t test. (**D**) Glutamate-induced inward current in whole-cell recorded axon blebs. (**E**) Phase-space analysis of an eAP waveform. (Left) An eAP was plotted in the space of V versus dV/dt, where V represents the eAP voltage at a given time. The phase θ (blue arrow) was determined to maximize the difference between the orbits of eAPs before (black) and during drug application (red). Right: The θ values were similar for eAPs modulated by glutamate, high-K^+ depolarization, or 4-AP, but not by TTX. $n = 4$ or 5 slices.

modulate APs by depolarizing axons through AMPA receptor activation rather than by triggering transmitter release or Ca^{2+}-dependent cellular signals. Consistent with this, 20 mM K^+ applied to axons induced eAP broadening (Fig. 1C, t_3 = 4.59, P = 0.0037).

In CA3 PCs of acute hippocampal slices, the cut ends (blebs) of the axons were whole-cell patch-clamped (*2*). Puffing glutamate to the blebs elicited an inward current of 38.2 ± 5.6 pA at a holding potential of –70 mV (Fig. 1D, n = 3 blebs).

To investigate the mechanisms underlying the AP broadening, we analyzed the eAP waveform in the phase space of V versus dV/dt (Fig. 1E). The orbits of control and glutamate-broadened eAPs separated maximally in a late phase during their temporal evolution. The late-phase modulation was replicated by high-K^+ depolarization and pharmacological blockade of the Kv1 family of voltage-activated K^+ channels by 10 μM 4-aminopyridine (4-AP), whereas the earlier phase was sensitive to partial blockade of voltage-activated Na^+ channels by 10 nM tetrodotoxin (TTX). Thus, depolarization-induced K^+ channel inactivation (*1*, *4*) is likely to underlie the AP broadening.

To determine the extent of glutamate's influence, we patched axons at various distances downstream of the site of glutamate administration. eAP broadening was more evident at axons nearer the site of glutamate administration, and the decay constant was found to be 223 μm (Fig. 2A, n = 17 axons). Likewise, the eAP-broadening effect was not observed at distances greater than 250 μm upstream from the glutamate spot (t_4 = 0.51, P = 0.60) or at axon branches other than those that received glutamate puffs (Fig. 2B, t_5 = 0.66, P = 0.54).

Adenosine A_1 receptors are expressed in presynaptic axons (*9*). Local application of 1 mM adenosine did not modulate eAPs (Fig. 1C, t_5 = 0.33, P = 0.75), but 100 μM 8-cyclopentyl-1,3-dipropylxanthine (DPCPX), an A_1 receptor antagonist, increased the eAP width (Fig. 1C, t_5 = 7.61, P = 0.0006), suggesting tonic AP suppression by endogenous adenosine.

We next sought to determine whether AP modulation affects presynaptic Ca^{2+} dynamics (fig. S3). Oregon Green BAPTA-1 (OGB1), a Ca^{2+} indicator, was intracellularly injected into PCs. In some cases, its AM form was bolus-injected into the stratum oriens. Intra-axonally diffused dye was confocally imaged from individual presynaptic boutons. APs induced a transient rise in Ca^{2+} fluorescence in the boutons. The increases in Ca^{2+} were further enhanced by glutamate applied to axons. This enhancement did not occur in the presence of CNQX and AP5. DPCPX, but not adenosine, also enhanced the Ca^{2+} response.

To investigate whether AP broadening modulates synaptic efficacy, we recorded synaptically connected pairs of CA3 PCs. In each experiment, we identified the axon branch that was responsible for the synaptic connection by sequentially puffing 1 μM TTX onto individual Alexa-visualized axon collaterals (Fig. 3A). Focal activation of the identified branch by glutamate application increased the mean amplitude of unitary excitatory postsynaptic currents (uEPSCs) in the downstream postsynaptic neurons (Fig. 3, B and C, t_{11} = 3.49, P = 0.006) and decreased the failure of synaptic transmission (fig. S4) and the paired-pulse response ratio (PPR), defined as the second uEPSC amplitude divided by the first evoked by two 50-ms-interval stimuli (Fig. 3D, t_4 = 4.31, P = 0.01). DPCPX (Fig. 3D, t_5 = 5.70, P = 0.002), but not adenosine (Fig. 3D, t_5 =1.38, P = 0.23), increased the uEPSC amplitude. 4-AP also increased synaptic efficacy (Fig. 3D, t_5 = 5.46, P = 0.003) and decreased PPR (t_5 = 7.81, P = 0.0006).

Most local axons of CA3 PCs are unmyelinated, and their shafts and presynaptic varicosities contact astrocytes (*10*). These periaxonal astrocytes may modulate APs through the release of gliotransmitters. Astrocytes residing near the axons of CA3 PCs (150 to 400 μm from axon

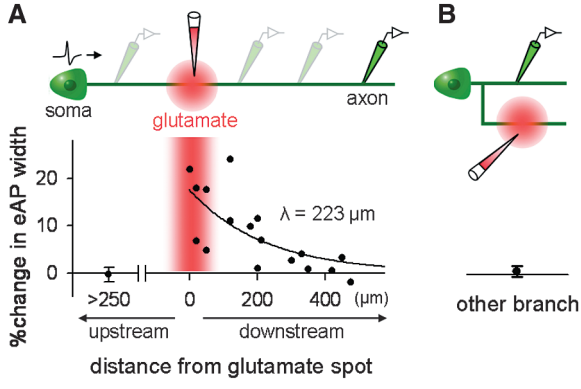

Fig. 2. The AP-broadening effect reaches beyond the glutamate-activated region. **(A)** A glutamate-induced increase in axonal eAP width is plotted against the path distance between the glutamate puff and the cell-attached recording positions. Red indicates the puffed area (<100 μm ϕ). The line was best fit to a single exponential decay (R^2 = 0.50, P = 0.01, n = 17 axon recordings). The decay constant λ (223 μm) was smaller than the axon length constant reported previously (~500 μm) (*2*–*4*). Extracellular recording of APs may underestimate the effect of AP broadening. **(B)** Glutamate applied to axon branches in different locations than the recording site had no effect. n = 6 axons.

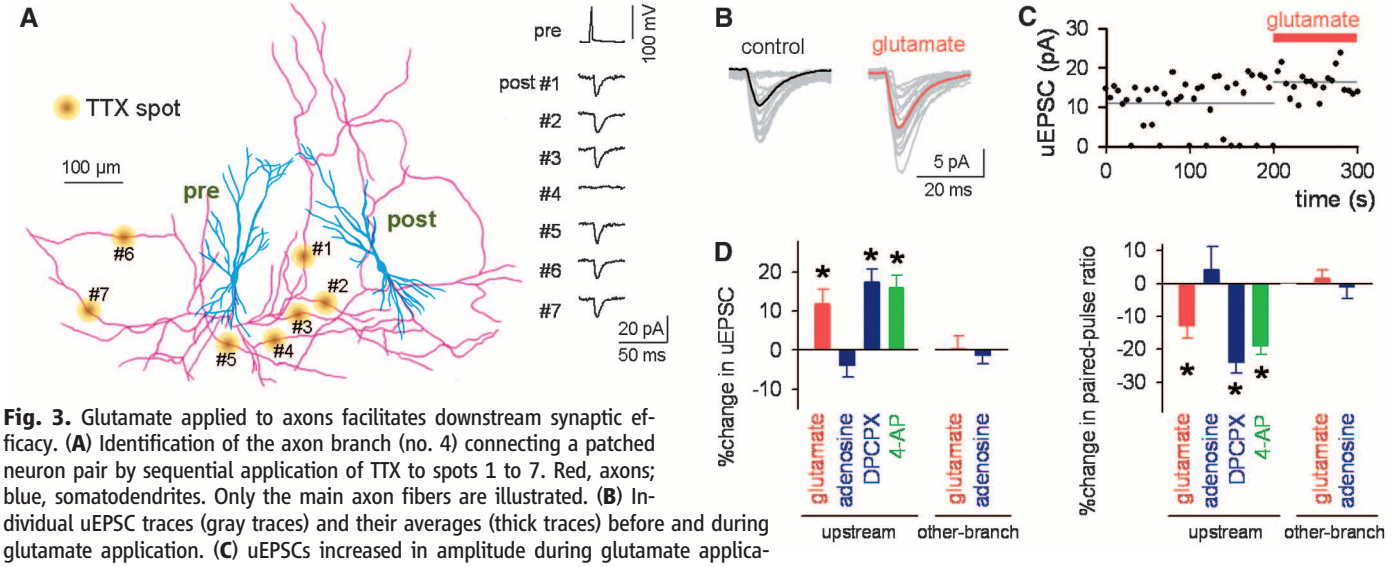

Fig. 3. Glutamate applied to axons facilitates downstream synaptic efficacy. **(A)** Identification of the axon branch (no. 4) connecting a patched neuron pair by sequential application of TTX to spots 1 to 7. Red, axons; blue, somatodendrites. Only the main axon fibers are illustrated. **(B)** Individual uEPSC traces (gray traces) and their averages (thick traces) before and during glutamate application. **(C)** uEPSCs increased in amplitude during glutamate application. **(D)** Effects of local drug application on synaptic responses evoked by single-pulse (left) and paired-pulse (right) stimulation. n = 5 to 12 slices, *P < 0.05, paired t test.

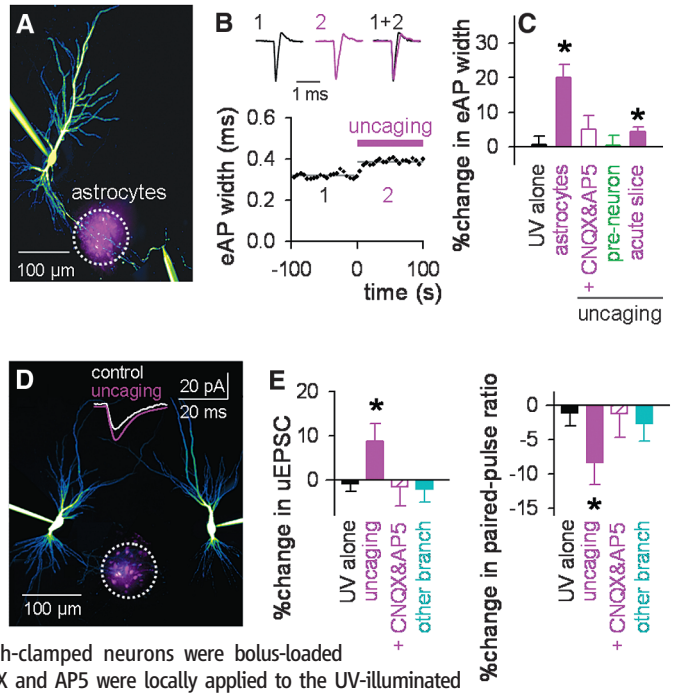

Fig. 4. Ca^{2+} uncaging in periaxonal astrocytes broadens APs and facilitates downstream synaptic transmission. (**A**) Astrocytes (magenta) bolus-loaded with NP-EGTA-AM near the axon whose soma and downstream axon (green) were patch-clamp–recorded. UV illuminated the circled area. (**B**) Photolysis of NP-EGTA induced axonal eAP broadening. Inset at top: eAPs at time points 1 and 2. (**C**) Summarized data, including slices that were not loaded with NP-EGTA-AM (UV alone) and slices in which the presynaptic neuron was intracellularly loaded with NP-EGTA (pre-neuron). (**D**) Astrocytes near the axon connecting two patch-clamped neurons were bolus-loaded with NP-EGTA-AM. (**E**) CNQX and AP5 were locally applied to the UV-illuminated area. UV was also applied to unloaded slices (UV alone) and slices in which NP-EGTA-AM was bolus-loaded into the astrocytes around irrelevant axon branches (other branch). $n = 6$ to 19 slices, $^*P < 0.05$, paired t test.

hillocks) were bolus-loaded with OGB1-AM and *O*-nitrophenyl-ethylene glycol tetraacetic acid AM (NP-EGTA-AM), a membrane-permeating caged-Ca^{2+} compound (Fig. 4A). Astrocytes were morphologically and immunohistochemically identified (fig. S5) and preferentially loaded with NP-EGTA-AM (*11*). Photolysis of caged Ca^{2+} by an ultraviolet (UV) pulse (120 μm in diameter) elicited oscillatory Ca^{2+} fluctuations in the illuminated astrocytes, which persisted for several minutes (fig. S6D). The activity did not propagate to neighboring, nonilluminated astrocytes. UV illumination did not activate astrocytes that were not loaded with NP-EGTA (fig. S6E, UV alone).

Ca^{2+} uncaging in astrocytes increased the duration of eAPs recorded at downstream axons within 200 μm of the UV spot (Fig. 4, B and C, $t_6 = 5.90$, $P = 0.001$). The same effect was observed in axons of CA3 PCs of acute hippocampal slices (a 4.5 ± 1.0% increase in eAP width, $t_3 = 4.83$, $P = 0.02$). UV pulses did not induce eAP broadening in the presence of CNQX and AP5 (Fig. 4C, $t_4 = 1.40$, $P = 0.23$) or in slices without NP-EGTA-AM loading (Fig. 4C, $t_4 = 0.38$, $P = 0.73$). We rule out the possibility that UV-induced Ca^{2+} elevation in NP-EGTA–loaded axons caused the eAP broadening, because UV illumination of axons of presynaptic neurons injected with 200 μM NP-EGTA failed to broaden eAPs (Fig. 4C, $t_4 = 0.02$, $P = 0.98$). Astrocyte activation increased the amplitude of AP-triggered Ca^{2+} transients in presynaptic boutons, an effect that was not observed in the presence of CNQX and AP5 or in slices without NP-EGTA loading (fig. S7).

To examine whether the Ca^{2+} activity of periaxonal astrocytes facilitated downstream synaptic efficacy, astrocytes near the presynaptic axon branches connecting patched PC pairs were loaded with NP-EGTA-AM (Fig. 4D). UV activation of these astrocytes amplified uEPSCs in the postsynaptic neurons (Fig. 4E, $t_{18} = 2.27$, $P = 0.03$) and reduced PPR ($t_{15} = 2.54$, $P = 0.02$). Both effects were blocked by coapplication of CNQX and AP5 to the UV-illuminated area (Fig. 4E, $t_8 = 0.24$, $P = 0.81$). Neither UV illumination alone (Fig. 4E, $t_9 = 0.97$, $P = 0.36$) nor UV activation of astrocytes on irrelevant axon branches ($t_5 = 0.82$, $P = 0.45$) facilitated synaptic transmission. To examine the impact of single astrocyte activation, we injected NP-EGTA into a periaxonal astrocyte through a whole-cell pipette (fig. S8A). In 5 of 13 experiments, photostimulation led to a modest but significant increase in uEPSC efficacy as well as a decrease in PPRs. When the data for the entire sample were analyzed statistically, these effects were still significant (fig. S8B). Ca^{2+} uncaging in the axons of NP-EGTA–loaded presynaptic neurons failed to modulate synaptic transmission.

We demonstrated that activation of AMPA receptors directly or indirectly causes a depolarizing current in axons and thereby broadens APs during axonal conduction. The endogenous agonist glutamate appears to be provided by periaxonal astrocytes [but see (*12*)]. Astrocytes are known to regulate local synaptic transmission (*13*–*16*), but this work reveals that they are far more influential than expected, because the length constant of the axon cable (*2*–*4*) exceeds their cell diameter. Our findings derived from experimentally designed ex vivo systems using artificial stimulation should be extrapolated to other systems with caution. Elucidating their physiological relevance requires further investigation.

References and Notes

1. Y. Shu, Y. Yu, J. Yang, D. A. McCormick, *Proc. Natl. Acad. Sci. U.S.A.* **104**, 11453 (2007).
2. Y. Shu, A. Hasenstaub, A. Duque, Y. Yu, D. A. McCormick, *Nature* **441**, 761 (2006).
3. H. Alle, J. R. Geiger, *Science* **311**, 1290 (2006).
4. M. H. Kole, J. J. Letzkus, G. J. Stuart, *Neuron* **55**, 633 (2007).
5. K. W. Schicker, M. M. Dorostkar, S. Boehm, *Curr. Mol. Pharmacol.* **1**, 106 (2008).
6. H. S. Engelman, A. B. MacDermott, *Nat. Rev. Neurosci.* **5**, 135 (2004).
7. Materials and methods are available as supporting material on *Science* Online.
8. D. Ishikawa *et al.*, *Neural Netw.* **23**, 669 (2010).
9. R. A. Cunha, *Neurochem. Int.* **38**, 107 (2001).
10. R. Ventura, K. M. Harris, *J. Neurosci.* **19**, 6897 (1999).
11. Q. S. Liu, Q. Xu, G. Arcuino, J. Kang, M. Nedergaard, *Proc. Natl. Acad. Sci. U.S.A.* **101**, 3172 (2004).
12. N. B. Hamilton, D. Attwell, *Nat. Rev. Neurosci.* **11**, 227 (2010).
13. J. Kang, L. Jiang, S. A. Goldman, M. Nedergaard, *Nat. Neurosci.* **1**, 683 (1998).
14. P. Jourdain *et al.*, *Nat. Neurosci.* **10**, 331 (2007).
15. G. Perea, A. Araque, *Science* **317**, 1083 (2007).
16. C. Henneberger, T. Papouin, S. H. Oliet, D. A. Rusakov, *Nature* **463**, 232 (2010).

17. This work was supported in part by a Grant-in-Aid for Science Research (nos. 22115003, 22650080, and 22680025) from the Ministry of Education, Culture, Sports, Science, and Technology of Japan. T.S. collected experimental data and carried out the data analysis. Y.I. conceived the project and carried out the data analysis. T.S. and Y.I. wrote the manuscript. N.M. supervised the project and provided feedback on the manuscript.

Supporting Online Material

www.sciencemag.org/cgi/content/full/331/6017/599/DC1
Materials and Methods
Figs. S1 to S8
References

9 September 2010; accepted 29 December 2010
10.1126/science.1197598

Action Potential Modulation during Axonal Conduction

Takuya Sasaki, Norio Matsuki, and Yuji Ikegaya

Contents

1. Methods
   1.1 Hippocampal slice cultures
   1.2 Acute hippocampal slices
   1.3 Electrophysiological recordings
   1.4 Calcium imaging and calcium uncaging
   1.5 Pharmacology
   1.6 Immunohistochemistry

2. Acknowledgments

3. References

4. Supporting Figures
   Figure S1 Comparison of intracellularly and extracellularly recorded APs
   Figure S2 Local glutamate application does not change the activity of the entire network
   Figure S3 Glutamate applied to axons increases the amplitude of AP-evoked calcium responses in downstream presynaptic boutons
   Figure S4 Glutamate application to presynaptic axon shafts increases synaptic efficacy and potency and decreases failure rate.
   Figure S5 Histochemical identification of astrocytes
   Figure S6 UV-evoked uncaging of NP EGTA induces calcium activity in astrocytes in the UV-illuminated region
   Figure S7 Activation of peri-axonal astrocytes increases the amplitude of AP-evoked calcium responses in presynaptic boutons
   Figure S8 Activation of peri-axonal astrocytes facilitates synaptic transmission

1. Methods

All experiments were performed with the approval of the animal experiment ethics committee at the University of Tokyo (approval number, 19-37 and 19-39) and according to the University of Tokyo guidelines for the care and use of laboratory animals. Data are summarized as the means ± standard errors. For all statistics, the paired-*t* test was used to compare data that were collected 'before' and 'during' axon stimulation.

1.1 Hippocampal slice cultures. Unless otherwise specified, we used organotypic slice culture preparations because these tissues are more transparent than acute slice preparations and are suitable for axon visualization and uncaging by ultraviolet (UV) light. Postnatal day 7 Wistar/ST rats were chilled with ice and decapitated. The brains were removed and horizontally cut using a vibratome into 300-μm-thick slices in aerated, ice-cold physiological saline supplemented with 25 mM glucose. Entorhino-hippocampal stumps were cultivated for 7–14 days on membrane filters (φ25 mm) (*1*). Cultures were fed with 50% minimal essential medium, 25% Hanks' balanced salt solution, and 25% horse serum in a humidified incubator at 37°C in 5% CO_2. The medium was changed every 3.5 days.

1.2 Acute hippocampal slices. In Figures 1D and E and in some experiments with calcium uncaging in astrocytes, we used acute slice preparations. Postnatal 7-to-12-day-old Wistar/ST rats (SLC, Shizuoka, Japan) were anesthetized with ether and decapitated. The brain was immersed in ice-cold modified artificial cerebrospinal fluid (aCSF) consisting of (in mM) 27 $NaHCO_3$, 1.4 NaH_2PO_4, 2.5 KCl, 0.5 ascorbic acid, 7.0 $MgSO_4$, 1.0 $CaCl_2$, and 222 sucrose bubbled with 95% O_2 and 5% CO_2. Horizontal entorhino-hippocampal slices of 400 μm thickness were cut using a vibratome and

maintained for more than 60 min at room temperature in normal aCSF consisting of (in mM) 123 NaCl, 26 $NaHCO_3$, 2.2 KCl, 1.24 NaH_2PO_4, 3.0 $MgSO_4$, 3.0 –3.2 $CaCl_2$, and 10 glucose and then bubbled with 95% O_2-5% CO_2.

1.3 Electrophysiological recordings. Slices were mounted in a recording chamber at 32ºC and perfused at a rate of 1.5–3 ml/min with aCSF bubbled with 95% O_2-5% CO_2. Patch-clamp recordings were collected from somata and axons with an amplifier and a digitizer that were controlled by pCLAMP 10 software. For somatic recording, borosilicate glass pipettes (5–7 MΩ) were filled with an internal solution consisting of (in mM) 135 K-gluconate, 4 KCl, 10 HEPES, 10 phosphocreatine-Na_2, 0.3 Na_2-GTP, and 4 Mg-ATP (pH 7.2). The whole-cell configuration was maintained for 1–2 hours to visualize axon morphology. Axonal cell-attached recording was conducted with fluorophore-coated pipettes (*2*). The tip of a glass pipette (9–12 MΩ) was immersed for 5–10 s in 0.02% bovine serum albumin Alexa Fluor 488 conjugate in 0.1 M phosphate-buffered saline. Signals were low-pass filtered at 1–2 kHz, digitized at 20-100 kHz, and analyzed with pCLAMP 10 software. APs were evoked by current injections (2–3 ms, 1–2 nA). When patching neurons, 200 μM Alexa Fluor 488 hydrazide was added to the intra-pipette solution to visualize cell morphology. When patching astrocytes, 100 μM OGB1 potassium salt, 200 μM NP-EGTA, 2% biocytin, and 10 mM glucose were added to the pipette solution. Astrocytes were identified under differential interference contrast microscopy. This morphological identification was verified by post-hoc immunohistochemistry with S100β, an astrocyte marker (Fig. S5). In acute slices, whole-cell recordings were obtained from the cut end of the axon (bleb). A glass pipette (15-20 MΩ) filled with the intracellular solution was advanced to the axon bleb under a differential interference contrast microscope equipped with a 40×

water immersion objective and a 2× optical magnifier. Data were discarded if access resistance changed by more than 20% during an experiment. The blebs were identified as axons based on the morphology and *en passant* synaptic varicosities of fibers retrogradely traced by Alexa Fluor 488.

1.4 Calcium imaging and calcium uncaging. For calcium imaging and uncaging in astrocytes, a glass pipette (4–6 MΩ) for dye loading was filled with aCSF that consisted of 50 μM OGB1-AM, 100 μM NP-EGTA-AM, 15% Pluronic F-127, and 10% DMSO. The tip of the pipette was inserted into the stratum oriens and the dye solution was injected by manually controlling a 10-ml syringe pressurizer (50–60 hPa for 3–5 min) (*3*). After a recovery period of >15 min in a recording chamber that was perfused with aCSF, images were captured at 1 frame per s (fps) with Nipkow-disk confocal microscopy, a cooled CCD camera, and an upright microscope with a water-immersion objective lens (16×, 0.8 numerical aperture or 40×, 0.9 numerical aperture). The OGB1 fluorescence was excited at 488 nm with a laser diode and visualized with a 507 nm long-pass emission filter. Astrocytes were identified by their morphology and calcium dynamics (*4*). NP-EGTA was uncaged by a 150-μm-diameter UV pulse for 30–120 s. UV light was emitted from a 100 mW high-pressure mercury lamp and short-passed at 330 nm. For multineuron calcium imaging (Fig. S2), a dye-loaded glass pipette was inserted into the CA3 stratum pyramidale and the dye was injected with a pressure of 50–60 hPa for 5 min. To facilitate spontaneous activity, the recording chamber was perfused with modified aCSF consisting of the following (in mM): 127 NaCl, 26 $NaHCO_3$, 3.3 KCl, 1.24 KH_2PO_4, 1.0 $MgSO_4$, 1.0 $CaCl_2$, and 10 glucose (*4*). Images were captured at 10 fps. For calcium imaging from single axons (Fig. S3A), 200 μM OGB1 potassium salt was intracellularly injected into single pyramidal cells through

patch-clamp pipettes. Recordings (100 fps) were carried out on synaptic varicosities 150–200 μm from the soma. For axonal calcium imaging in Figures S3B-D, a dye-loaded glass pipette was inserted into the CA3 stratum oriens and the dye was injected with a pressure of 50–60 hPa for 30-60 min to allow intra-axonal diffusion. The same pipette was used as a field stimulation electrode, and single rectangular-pulse stimuli (50-μs duration at 100 μA) were applied at intervals of 30 s. Spike-induced calcium transients were imaged at 20-100 fps from synaptic varicosities 150–200 μm from the pipette. Local glutamate application may induce a change in the extracellular space due to swelling, but we did not observe glutamate-induced movement of axons in the imaged field, at least not at micrometer resolution.

1.5 Pharmacology. Adenosine, L,D-2-amino-5-phosphonopentanoic acid (AP5), 4-aminopyridine (4-AP), 1,2-bis(*o*-aminophenoxy)ethane-N,N,N',N'-tetraacetic acid (BAPTA), 6-cyano-7-nitroquinoxaline-2,3-dione (CNQX), 8-cyclopentyl-1,3-dipropylxanthine (DPCPX), (S)-α-methyl-4-carboxyphenylglycine (MCPG), tetanus toxin (TeNT), tetrodotoxin, and DL-threo-β-benzyloxyaspartic acid (TBOA) were used. These agonists and inhibitors were dissolved immediately before use. To stimulate axons, 1 mM adenosine, 10 μM 4-AP, 100 μM DPCPX, 10 μM glutamate, 1 mM GABA, 20 mM potassium chloride solution, and 1 μM tetrodotoxin were pressure-applied locally through glass pipettes (5–7 MΩ). This pressure was adjusted so that the effective radius of this local application was less than 100 μm as confirmed by diffusion of co-applied Alexa Fluor dye (*5*). Because Alexa Fluor dye, unlike neurotransmitters, is not rapidly taken up by glia and neurons, this radius may be overestimated, and our local application procedure was more strictly limited than our estimation. The direction of the local puff was set to the same as the aCSF flow in the

chamber, which was roughly vertical to the longitudinal axis of axons of interest. In Figures 1C, 1E and 4C, 50 μM AP-5, 10 μM CNQX, 500 μM MCPG, and 100 μM TBOA were bath applied. In experiments with TeNT (Figure 1C), slices were preincubated with 10 nM TeNT for 120 min before the recording session. The effectiveness of TeNT was confirmed by a lack of spontaneous synaptic inputs in patched neurons. In Figure 1C, 20 mM BAPTA was intracellularly injected into neuronal cell bodies through whole-cell patch-clamp pipettes. In Figure 4E, 10 μM CNQX and 50 μM AP5 were locally applied to the area of UV illumination.

1.6 Immunohistochemistry. Astrocytes were *post hoc* labeled with biocytin-streptavidin Alexa-568 conjugate and S100β immunostaining. After recording, slices were fixed in 4% paraformaldehyde in 0.1 M phosphate buffer solution for 2 h and permeabilized with 0.3% Triton X-100 for 60 min. After being blocked by a 60-min incubation with 2% goat serum at 4°C, they were incubated with Alexa Fluor 568-conjugated streptavidin and primary rabbit monoclonal anti-S100β antibody overnight at 4°C and labeled with secondary anti-rabbit IgG Alexa-488 for 2 h at room temperature.

2. Acknowledgments

We are grateful to Dr. Junya Ichikawa and Dr. Takeshi Toyoda for technical support for immunostaining and electrophysiology and to all lab members for continuing assistance.

3. References

1. R. Koyama *et al.*, *J Pharmacol Sci* **104**, 191 (2007).

2. D. Ishikawa *et al.*, *Neural Netw* **23**, 669 (2010).

3. T. Sasaki, G. Minamisawa, N. Takahashi, N. Matsuki, Y. Ikegaya, *J Neurophysiol* **102**, 636 (2009).

4. T. Sasaki, N. Matsuki, Y. Ikegaya, *J Neurosci* **27**, 517 (2007).

5. R. X. Yamada *et al.*, *J Neurosci* **28**, 4613 (2008).

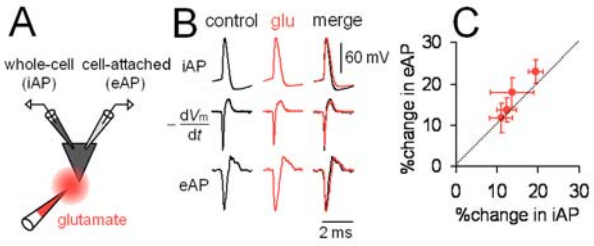

Fig. S1. Comparison of intracellularly and extracellularly recorded APs. (**A**) Simultaneous whole-cell and cell-attached recordings from the somata of single CA3 pyramidal cells. Glutamate (10 μM) was applied to the soma through another pipette. (**B**) Typical traces of intracellularly recorded action potentials (iAP, top), the first derivative of the iAP traces ($-dV_m/dt$, middle), and extracellularly recorded action potentials (eAP, bottom) before (black) and during glutamate application (red). Extracellularly recorded APs (eAPs) are theoretically believed to correspond to the first derivative of intracellularly recorded APs (iAPs) under biophysically ideal conditions. However, under actual experimental conditions, eAPs were more likely a mixture of negative iAPs and their derivatives. (**C**) Linear relationship of glutamate-induced changes in AP width between iAPs and eAPs. $n = 4$ cells, each averaged over 20 trials ($R = 0.89$, $P = 6.2 \times 10^{-7}$).

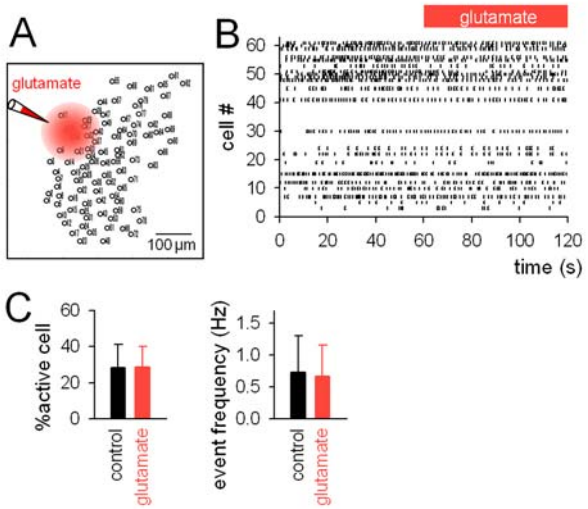

Fig. S2. Local glutamate application does not change the level of network activity. (**A**) Positions of 62 arbitrarily numbered neurons (open circles) and estimated area of glutamate application (shaded circle). (**B**) Rastergram representing the spatiotemporal pattern of spontaneous calcium events of the 62 neurons. Each dot represents the onset time of a single calcium transient of the corresponding neuron. Ten µM glutamate was applied during the period between 60 and 120 s (**C**) Glutamate application did not affect the ratio of active cells to total cells recorded (left; $t_3 = 0.34$, $P = 0.76$) or the mean frequency of neuronal calcium events (right; $t_3 = 1.32$, $P = 0.28$). $n = 4$ slices, including 291 cells, paired *t*-test.

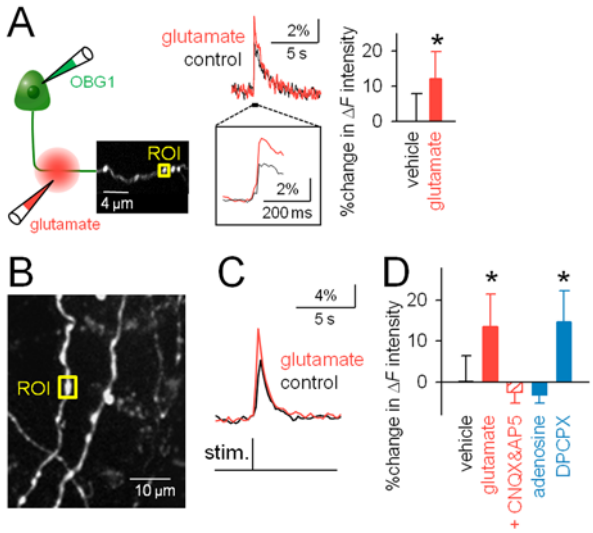

Fig. S3. Glutamate applied to axons increases the amplitude of AP-evoked calcium responses in downstream presynaptic boutons. (**A**) OGB1 potassium salt (200 μM) was intracellularly injected into a single pyramidal cell through a patch-clamp pipette (left). Recordings were carried out from synaptic varicosities 150–200 μm from the soma. The calcium intensity was measured at 100 Hz from the varicosity indicated by the region of interest (ROI). Action potentials induced a fast calcium transient. Ten successive trials were averaged. The inset shows the time expansion (100×) of the part indicated by the bar under the calcium traces, indicating that glutamate application increased the amplitude of calcium transients. The bar graph summarizes glutamate-induced (red) and vehicle-induced (black) changes in the amplitude of AP-evoked calcium transients. Glutamate increased the amplitude (t_4 = 5.49, P = 0.0054). The local application of glutamate by itself did not induce movement of the imaged axons. n = 4 slices. (**B**) OGB1-AM was pressure-injected into the CA3 stratum oriens to label presynaptic fibers, and calcium responses to APs that were evoked by a single pulse of field stimulation to the stratum oriens were monitored 20 Hz from individual presynaptic boutons. (**C**) Representative calcium fluorescence traces before and during glutamate application. Five successive trials were averaged. (**D**) Changes in the amplitude of AP-evoked calcium transients after the application of glutamate, adenosine, and DCPCX. The calcium amplitude increased when glutamate was applied to axons (t_5 = 2.58, P = 0.049). This enhancement of the calcium dynamics did not occur in the presence of CNQX and AP5 (t_4 = 1.07, P = 0.34). DPCPX, but not adenosine, enhanced the calcium responses (DPCPX: t_5 = 3.05, P = 0.03; adenosine: t_6 = 1.67, P = 0.15). n = 6–7 slices, including 10 boutons each. *P < 0.05, paired-t test.,

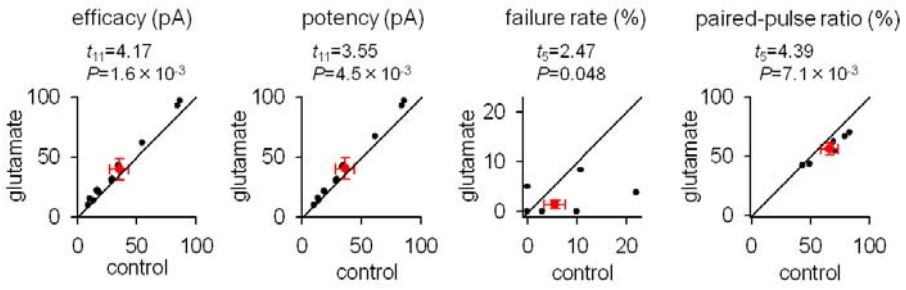

Fig. S4. Glutamate application to presynaptic axon shafts increases synaptic efficacy (left) and potency (middle left) but decreases failure rate (middle right) and paired pulse response ratios (right). Each dot indicates the data obtained for a single pair recording, and red dots are the means ± standard errors (n = 6−12 slices). The line indicates the diagonal. Synaptic efficacy is the mean amplitude of the uEPSCs for all trials, including the failed transmission trials, and the synaptic potency is the mean uEPSC amplitude at successful transmission trials. The failure rate is the percentage of the number of failure transmission trials among the total trial number.

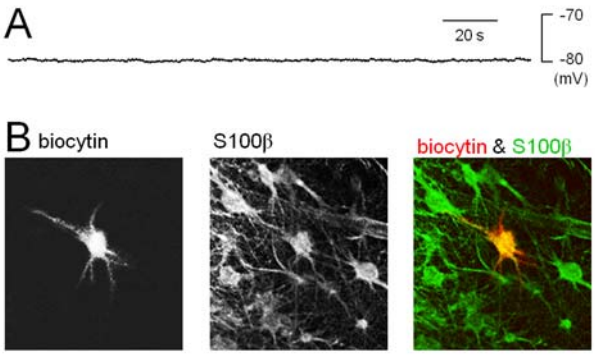

Fig. S5. Immunohistochemical identification of astrocytes. In this study, astrocytes were morphologically identified using differential interference contrast microscopy. In some experiments, the cells were *post hoc* labeled with S100β immunostaining. We confirmed that all selected cells were S100β-positive. (**A**) Whole-cell recording from an indentified astrocyte. The membrane potential was about -80 mV and did not spontaneously fluctuate due to synaptic inputs. (**B**) S100β immunoreactivity of an astrocyte that was identified and given an intracellular injection of biocytin.

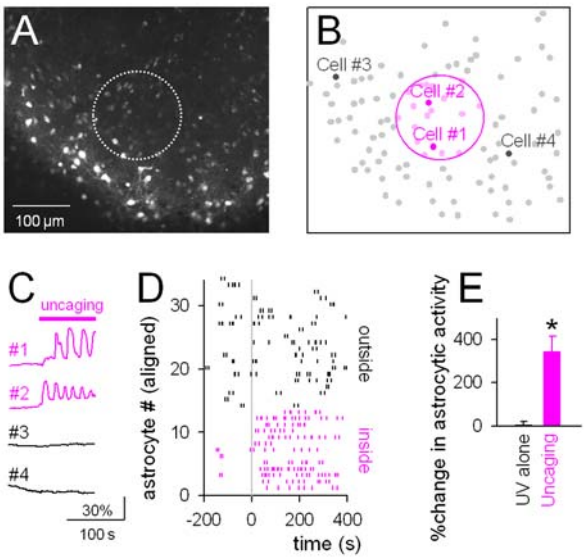

Fig. S6. UV-evoked uncaging of NP EGTA induces calcium activity in astrocytes in the UV-illuminated region. (**A**) Confocal images of a slice incubated with OGB1-AM and NP-EGTA-AM. The circle indicates the UV-illuminated zone. (**B**) OGB1-labeled astrocytes were selected for fluorescence measurement (gray dots). (**C**) The calcium responses of four representative cells (numbered in **B**) to UV illumination. **(D**) Representative rastergram of astrocytic activities following UV illumination. Each dot indicates a single calcium-increase event. The activity frequency increased in astrocytes within (but not outside, black) the illuminated region (red). (**E**) UV light induced an uncaging of calcium that elevated the activity frequency of the astrocytes. UV illumination had no effect on slices that were incubated in the absence of NP-EGTA-AM (UV alone). $n = 13$ slices each. *$p < 0.05$, paired-t test.

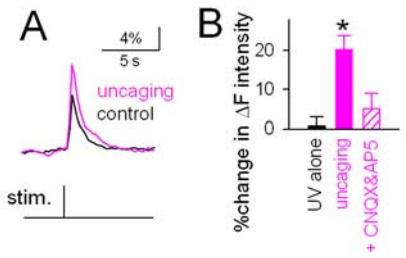

Fig. S7. Activation of peri-axonal astrocytes increases the amplitude of AP-evoked calcium responses in downstream presynaptic boutons. OGB1-AM was pressure-injected into the CA3 stratum oriens to label presynaptic fibers, and calcium responses to APs that were evoked by a single pulse of field stimulation were monitored from individual presynaptic boutons. Peri-axonal astrocytes 150-200 μm upstream of the imaged axons were bolus-loaded with NP-EGTA-AM. (**A**) Representative calcium fluorescence traces before and after UV uncaging. Five successive trials were averaged. (**B**) Summarized data for changes in the amplitude of AP-evoked calcium transients. CNQX and AP5 were locally applied to NP-EGTA-AM-injected regions. Astrocyte activation increased the amplitude of AP-triggered presynaptic calcium transients (t_4 = 3.78, P = 0.02). This effect was not observed in the presence of CNQX and AP5 (t_4 = 0.23, P = 0.83) or in slices without NP-EGTA-AM loading (t_3 = 0.09, P = 0.93). n = 4–5 slices, including 10 boutons each. *P < 0.05, paired-t test.

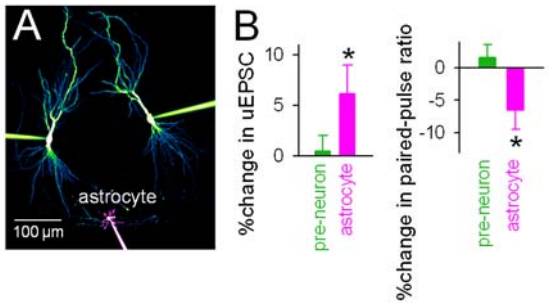

Fig. S8. Activation of single peri-axonal astrocytes facilitates synaptic transmission. (**A**) NP-EGTA-AM was injected into a single astrocyte (magenta) residing near an axon branch that connects synaptic neuron pairs (green, pre: right) (**B**) The uEPSC amplitude increased and the PPR decreased after UV uncaging of astrocytes (astrocyte; amplitude: $t_{12} = 2.21$, $P = 0.04$; PPR: $t_{11} = 2.28$, $P = 0.04$) but not presynaptic neurons (pre-neuron; amplitude: $t_9 = 0.24$, $P = 0.81$; PPR: $t_9 = 0.66$, $P = 0.52$). $n = 10$–14, $^*P < 0.05$, paired-t test.